

Naturalness and lepton number/ flavor violation in inverse seesaw models

Naoyuki Haba¹, Hiroyuki Ishida^{1,2}, and Yuya Yamaguchi^{1,3}

¹*Graduate School of Science and Engineering, Shimane University,
Matsue 690-8504, Japan*

²*Physics Division, National Center for Theoretical Sciences,
Hsinchu, Taiwan 300*

³*Department of Physics, Faculty of Science, Hokkaido University,
Sapporo 060-0810, Japan*

Abstract

We introduce three right-handed neutrinos and three sterile neutrinos, and consider an inverse seesaw mechanism for neutrino mass generation. From naturalness point of view, their Majorana masses should be small, while it induces a large neutrino Yukawa coupling. Then, a neutrinoless double beta decay rate can be enhanced, and a sizable Higgs mass correction is inevitable. We find that the enhancement rate can be more than ten times compared with a standard prediction from light neutrino contribution alone, and an analytic form of heavy neutrino contributions to the Higgs mass correction. In addition, we numerically analyze the model, and find almost all parameter space of the model can be complementarily searched by future experiments of neutrinoless double beta decay and $\mu \rightarrow e$ conversion.

1 Introduction

The experimental results on the neutrino oscillation have established an exact evidence of neutrino masses. Since the origin of neutrino masses cannot be explained within the standard model (SM), there are a lot of models towards explaining the tiny neutrino masses naturally. The type-I seesaw model [1] is one of the simplest idea, in which right-handed neutrinos are introduced. There is a large parameter space for their masses, and they could be solve some phenomenological problems: short baseline neutrino oscillation anomalies with a eV mass¹, relic abundance of dark matter with a keV mass, and baryon asymmetry of the universe (BAU) with GeV to TeV masses with a sufficient fine-tuning [see Ref. [11] for a review].

In the conventional type-I seesaw model, the tiny neutrino masses and the BAU can be simultaneously explained without a fine-tuning, in which the right-handed neutrinos are typically heavier than 10^9 GeV [12]. It is, however, impossible to search such heavy right-handed neutrinos directly. For the indirect searches, since the Majorana masses of right-handed neutrinos violate the lepton number conservation, lepton number violation processes might be detectable. Nevertheless, the absence of the neutrinoless double beta decay at the moment [13] suggests the approximate lepton number conservation. Then, the Majorana masses should be small from the naturalness in the sense of 't Hooft [14].

On the other hand, inverse seesaw models [15, 16, 17] are much interesting from experimental point of view. In the inverse seesaw models, there are right-handed neutrinos which couple with left-handed neutrinos and sterile neutrinos which do not couple with left-handed neutrinos. Compared with the type-I seesaw model, their Majorana masses can be smaller, which is preferred by the naturalness, and sizable neutrino Yukawa couplings are allowed. Thus, the inverse seesaw model has been strongly constrained by lepton flavor violations [18], cosmology [19] and collider experiments [20, 21]. Moreover, the inverse seesaw model can be highly testable by precise measurements of lepton flavor violation (for example, $\mu \rightarrow e\gamma$ [22], $\mu \rightarrow eee$ [23], and $\mu \rightarrow e$ conversion [24]), and high energy collider experiments [25]-[29]. In this paper, we focus on the (3, 3) inverse seesaw model, in which the number of both right-handed neutrinos and sterile neutrinos are three, and we do not consider the phenomenological issues mentioned above.

This paper is organized as follows. In Sec. 2, we briefly review the inverse seesaw mechanism and define our setup. In Sec. 3, we investigate heavy neutrino contributions for the neutrinoless double beta decay, and find an analytic form of the heavy neutrino contribution to the effective neutrino mass. In Sec. 4, we also investigate the Higgs mass correction coming from heavy neutrinos, which should be not so larger than the

¹ The neutrino oscillation anomalies have been reported by some experiments: reactor [2, 3, 4], accelerator [5]-[8] and Gallium [9, 10].

electroweak (EW) scale from the naturalness point of view. In Sec. 5, we show numerical results of heavy neutrino contributions to the effective neutrino mass and the Higgs mass correction. Finally, we summarize our results in Sec. 6.

2 Mass spectrum in inverse seesaw models

In this section, we explain a mass spectrum in inverse seesaw models. To realize the inverse seesaw mechanism, we introduce three vector-like gauge-singlet fermions, $\psi = \psi_L + \psi_R$ [see Ref. [30] for this setup]. The Lagrangian contains

$$\mathcal{L} = i\bar{\psi}\gamma^\mu\partial_\mu\psi - M_N\bar{\psi}\psi - \frac{\mu_L}{2}\bar{\psi}_L^c\psi_L - \frac{\mu_R}{2}\bar{\psi}_R^c\psi_R - Y_L\bar{\psi}_L^c\tilde{\Phi}^\dagger\ell - Y_R\bar{\psi}_R^c\tilde{\Phi}^\dagger\ell + \text{h.c.}, \quad (1)$$

where Φ and ℓ are the Higgs and lepton doublets, respectively, and $\tilde{\Phi}$ is the charge conjugation of Φ . The 3×3 complex matrices M_N , $\mu_{L,R}$, and $Y_{L,R}$ stand for vector-like mass, Majorana mass, and Yukawa coupling, respectively. Without loss of generality, rotating basis of vector-like fermions, the Lagrangian can be rewritten by

$$\mathcal{L} = i\bar{N}\gamma^\mu\partial_\mu N + i\bar{S}\gamma^\mu\partial_\mu S - M_N\bar{N}S^c - \frac{\mu_N}{2}\bar{N}^cN - \frac{\mu_S}{2}\bar{S}^cS - Y_\nu\bar{N}\tilde{\Phi}^\dagger\ell + \text{h.c.}, \quad (2)$$

where N and S are linear combinations of ψ_L^c and ψ_R . Here, $\mu_{N,S}$ and Y_ν are the 3×3 complex matrices corresponding to Majorana masses and neutrino Yukawa coupling, respectively. In the following, we consider this basis, in which S does not couple with L at tree level, and call N and S right-handed neutrino and sterile neutrino, respectively.

After the EW symmetry breaking, the Higgs obtains a nonzero vacuum expectation value, $\langle\Phi\rangle = v/\sqrt{2} \simeq 174 \text{ GeV}$, and then, the Dirac neutrino mass matrix is induced by $m_D = Y_\nu\langle\Phi\rangle$. Then, the 9×9 neutrino mass matrix is given by

$$\mathcal{M} = \begin{pmatrix} 0 & m_D^T & 0 \\ m_D & \mu_N & M_N \\ 0 & M_N^T & \mu_S \end{pmatrix}, \quad (3)$$

in the basis of $(\nu_L^c, N, S)^T$. The lepton number is broken by two Majorana masses μ_N and μ_S , and they should be much smaller than M_N and m_D in the 't Hooft's sense of naturalness. In the technically natural limit of $\mu_{N,S} \ll m_D, M_N$, the order of magnitude of mass eigenvalues are given by

$$\mathcal{O}(m_\nu) = \frac{m_D^2\mu_S}{m_D^2 + M_N^2} + \mathcal{O}(\mu_{N,S}^2), \quad (4)$$

$$\mathcal{O}(m_\pm) = \pm\sqrt{m_D^2 + M_N^2} + \frac{M_N^2\mu_S}{2(m_D^2 + M_N^2)} + \frac{\mu_N}{2} + \mathcal{O}(\mu_{N,S}^2). \quad (5)$$

In the limit of $\mu_{N,S} \rightarrow 0$, active neutrinos become massless and lepton number conservation is restored. Note that the active neutrino mass m_ν can be suppressed by small μ_S , but

does not depend on μ_N at the leading order. For $m_D \ll M_N$, the heavy neutrino masses are approximated by $\mathcal{O}(m_{\pm}) \simeq \pm M_N + (\mu_S + \mu_N)/2$, and thus, the mass difference between them is small as $\mathcal{O}(\mu_{N,S})$.

To explain the active neutrino mass scale $m_\nu \sim 0.1$ eV, if there is no accidental cancellation, or no fine-tuning, the energy scale of μ_S should be

$$\mu_S \sim \left(\frac{M_N}{1\text{TeV}} \right)^2 \left(\frac{1}{Y_\nu} \right)^2 \times 1\text{ eV}, \quad (6)$$

for a given M_N and Y_ν . Technically natural limit of $\mu_{N,S} \ll m_D, M_N$ requires

$$0.1\text{ eV} \lesssim \mu_S \ll 100\text{ GeV}, \quad (7)$$

where the lower and upper bounds have been obtained by $m_\nu \sim \mu_S(m_D/M_N)^2 \lesssim \mu_S$, and $m_D \lesssim 100\text{ GeV}$ corresponding to a perturbativity bound $Y_\nu \lesssim 1$, respectively. Using Eq. (6) and $Y_\nu \lesssim 1$, $M_N \ll 10^8\text{ GeV}$ is required to satisfy Eq. (7). Actually, μ_S and M_N are constrained more severely by the lepton flavor violation as we will show in Sec. 5.

In the matrix form, active neutrino mass matrix is given by

$$\begin{aligned} m_\nu &\simeq m_D^T (M_N^T)^{-1} \mu_S M_N^{-1} m_D \\ &= m_D^T X^{-1} m_D, \end{aligned} \quad (8)$$

where we have defined $X = M_N \mu_S^{-1} M_N^T$, and the last form is the same as the type-I seesaw model [1]. The active neutrino mass matrix is diagonalized by Pontecorvo-Maki-Nakagawa-Sakata (PMNS) matrix U_{PMNS} [31, 32]:

$$U_{\text{PMNS}}^T m_\nu U_{\text{PMNS}} = \text{diag}(m_1, m_2, m_3) \equiv D_m, \quad (9)$$

where m_i ($i = 1, 2$, and 3) are the mass eigenvalues of three lightest neutrinos. Actually, since this diagonalization is satisfied at leading order level, we will define an unitary matrix diagonalizing the full 9×9 neutrino mass matrix in the end of this section, and use it for numerical calculations.

Using the Casas-Ibarra parametrization [33], the neutrino Yukawa coupling matrix is parametrized by

$$Y_\nu = \frac{\sqrt{2}}{v} V^\dagger \sqrt{D_X} R \sqrt{D_m} U_{\text{PMNS}}^\dagger, \quad (10)$$

where V is a unitary matrix, which diagonalizes X by $V X V^T = \text{diag}(X_1, X_2, X_3) \equiv D_X$. The complex orthogonal matrix R can be parameterized by

$$R = \zeta \begin{pmatrix} c_{12}c_{13} & s_{12}c_{13} & s_{13} \\ -s_{12}c_{23} - c_{12}s_{23}s_{13} & c_{12}c_{23} - s_{12}s_{23}s_{13} & s_{23}c_{13} \\ s_{12}s_{23} - c_{12}c_{23}s_{13} & -c_{12}s_{23} - s_{12}c_{23}s_{13} & c_{23}c_{13} \end{pmatrix}, \quad (11)$$

where $c_{ij} = \cos \omega_{ij}$ and $s_{ij} = \sin \omega_{ij}$ with arbitrary complex angles ω_{ij} . The overall sign $\zeta = \pm 1$ ($\mathbf{1}$ is an 3×3 identity matrix) corresponds to degree of freedom of a parity transformation, which determines $\det[R] = \pm 1$ for $\zeta = \pm 1$. In the following, we assume that M_N , μ_S and μ_N are diagonal, and also $\mu_N = \mu_S$ for simplicity: $M_N = D_M \equiv \text{diag}(M_1, M_2, M_3)$ and $\mu_N = \mu_S = D_\mu \equiv \text{diag}(\mu_1, \mu_2, \mu_3)$. Then, $X = \text{diag}(X_1, X_2, X_3) = \text{diag}(M_1^2/\mu_1, M_2^2/\mu_2, M_3^2/\mu_3)$, and V becomes a unit matrix.

When both M_N and $\mu_{N,S}$ are diagonal, before the EW symmetry breaking, mass eigenvalues of heavy neutrinos become

$$m_{i\pm} = \pm M_i + \mu_i \quad \text{for } i = 1, 2, \text{ and } 3, \quad (12)$$

because of $m_D = 0$. The mass eigenvectors are given by $N_{i\pm} = (N_i \pm S_i)/\sqrt{2}$, and they have the same neutrino Yukawa couplings like $(Y_\nu/\sqrt{2})\overline{N}_{i\pm}\tilde{\Phi}^\dagger\ell$. Therefore, before the EW symmetry breaking, there exist the almost identical particles, which have the same couplings and masses with a small difference μ_i .

Since the degenerate heavy neutrinos naturally arise in inverse seesaw models, the BAU can be explained by leptogenesis through the neutrino oscillation [34, 35]. On the other hand, if the number of sterile neutrinos are larger than the number of right-handed neutrinos, there exist additional mass eigenstates with their masses of $\mathcal{O}(\mu_S)$. The new mass eigenstates can explain the short baseline neutrino oscillation anomalies with $\mu_S \sim \mathcal{O}(\text{eV})$ [36], and/or the relic density of dark matter with $\mu_S \sim \mathcal{O}(\text{keV})$ [37]. However, these issues are beyond the scope of this paper.

For the following discussion, it is useful to show the mass matrix in the $(\nu_L^c, N_{i\pm})^T$ basis:

$$\mathcal{M} = \begin{pmatrix} 0_{3 \times 3} & (m'_D)^T_{\alpha 1} & (m'_D)^T_{\alpha 1} & (m'_D)^T_{\alpha 2} & (m'_D)^T_{\alpha 2} & (m'_D)^T_{\alpha 3} & (m'_D)^T_{\alpha 3} \\ (m'_D)_{1\alpha} & m_{1-} & 0 & 0 & 0 & 0 & 0 \\ (m'_D)_{1\alpha} & 0 & m_{1+} & 0 & 0 & 0 & 0 \\ (m'_D)_{2\alpha} & 0 & 0 & m_{2-} & 0 & 0 & 0 \\ (m'_D)_{2\alpha} & 0 & 0 & 0 & m_{2+} & 0 & 0 \\ (m'_D)_{3\alpha} & 0 & 0 & 0 & 0 & m_{3-} & 0 \\ (m'_D)_{3\alpha} & 0 & 0 & 0 & 0 & 0 & m_{3+} \end{pmatrix}, \quad (13)$$

where $m'_D = m_D/\sqrt{2}$. Now, we define U as an unitary matrix diagonalizing this full 9×9 mass matrix, which is given in the following form:

$$U^T \mathcal{M} U = \mathcal{M}_{\text{diag}} \quad \text{with} \quad (\nu_e, \nu_\mu, \nu_\tau, N_{1-}, N_{1+}, N_{2-}, N_{2+}, N_{3-}, N_{3+})^T = U_{\alpha i} \nu_i. \quad (14)$$

The mass eigenstates ν_1, ν_2 and ν_3 correspond to the active neutrinos, and ν_i 's ($i = 4 \sim 9$) are the heavy neutrinos in light order from $i = 4$ to 9. For $m_D \ll M_N$, the heavy mass eigenstates are almost composed of $N_{i\pm}$. In particular, diagonal elements U_{ii} ($i = 4 \sim 9$)

are nearly unity, unless M_N is degenerate. In addition, matrix elements expressing the left-right mixing are almost satisfy $U_{\alpha 4}^2 \simeq U_{\alpha 5}^2$, $U_{\alpha 6}^2 \simeq U_{\alpha 7}^2$ and $U_{\alpha 8}^2 \simeq U_{\alpha 9}^2$ for $\alpha = e, \mu$ and τ , which are exactly satisfied in the limit of $\mu_i \rightarrow 0$.

3 Neutrinoless double beta decay

The massive Majorana neutrinos induce neutrinoless double beta decay, and its rate is proportional to the squared of the effective neutrino mass, which is given by

$$m_{\text{eff}} = \left| \sum_{i=1}^9 U_{ei}^2 \frac{\bar{p}^2}{\bar{p}^2 + m_i^2} m_i \right| \simeq \left| \left(\sum_{i=1}^3 U_{ei}^2 m_i \right) + m_{\text{eff}}^N \right|, \quad (15)$$

where $\bar{p}^2 \sim (200 \text{ MeV})^2$ is the typical virtual momentum of the neutrino. The first summation term corresponds to contributions from the active neutrinos, and m_{eff}^N stands for the heavy neutrino contributions. In the inverse seesaw model, m_{eff}^N can be obtained by [38]

$$\begin{aligned} m_{\text{eff}}^N &\simeq \sum_{i=1}^3 \left[-U_{e(2i+2)}^2 \frac{\bar{p}^2}{\bar{p}^2 + m_{i-}^2} |m_{i-}| + U_{e(2i+3)}^2 \frac{\bar{p}^2}{\bar{p}^2 + m_{i+}^2} |m_{i+}| \right] \\ &= - \sum_{i=1}^3 \left[(U_{e(2i+2)}^2 + U_{e(2i+3)}^2) \frac{[(M_i^2 - \mu_i^2) - \bar{p}^2] \bar{p}^2}{[(M_i^2 - \mu_i^2) + \bar{p}^2]^2 + 4\bar{p}^2 \mu_i^2} \mu_i \right. \\ &\quad \left. + (U_{e(2i+2)}^2 - U_{e(2i+3)}^2) \frac{[(M_i^2 - \mu_i^2) + \bar{p}^2] \bar{p}^2}{[(M_i^2 - \mu_i^2) + \bar{p}^2]^2 + 4\bar{p}^2 \mu_i^2} M_i \right]. \end{aligned} \quad (16)$$

In the limit of $\mu_i \rightarrow 0$ (no lepton number asymmetry), the heavy neutrino contributions exactly vanish due to $U_{e4}^2 = U_{e5}^2$, $U_{e6}^2 = U_{e7}^2$ and $U_{e8}^2 = U_{e9}^2$. Notice that we can usually take $(M_i^2 - \mu_i^2)^{1/2} \simeq M_i$, but this approximation becomes invalid if one considers leptogenesis thorough neutrino oscillations to explain the BAU, in which $0.1 \lesssim 2\mu_i/M_i \lesssim 1$ [35].

In addition, the unitary matrix U has the following approximate relations:

$$U_{\alpha(2i+2)}^2 + U_{\alpha(2i+3)}^2 \simeq \frac{(m_D^*)_{i\alpha}^2}{M_i^2} \quad \text{and} \quad U_{\alpha(2i+2)}^2 - U_{\alpha(2i+3)}^2 \simeq \frac{(m_D^*)_{i\alpha}^2}{M_i^2} \frac{2\mu_i}{M_i}, \quad (17)$$

where $\alpha = e, \mu$ and τ . Then, we find the analytic form of m_{eff}^N as

$$m_{\text{eff}}^N \simeq - \sum_{i=1}^3 \frac{\bar{p}^2}{(M_i^2 - \mu_i^2) + \bar{p}^2} \left[2 + \frac{(M_i^2 - \mu_i^2) - \bar{p}^2}{(M_i^2 - \mu_i^2) + \bar{p}^2} \right] (\tilde{m}_\nu^*)_{ie}, \quad (18)$$

with

$$(\tilde{m}_\nu)_{ie} = \frac{(m_D)_{ie}^2 \mu_i}{M_i^2}. \quad (19)$$

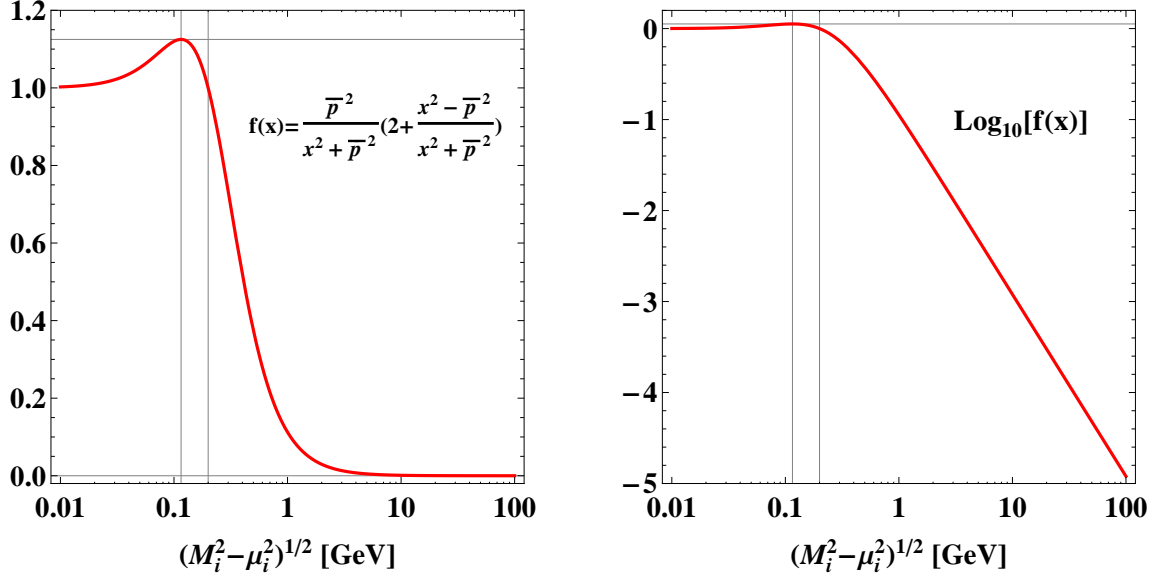


Figure 1: The suppression factor in Eq. (18). The vertical lines show $\sqrt{\bar{p}^2} = 200$ MeV and $\sqrt{\bar{p}^2/3}$. The horizontal line show $9/8$ as the maximal value. The right panel is shown with a logarithmic scale.

The coefficient factor in Eq. (18) is strongly suppressed for a large $(M_i^2 - \mu_i^2)^{1/2}$. Figure 1 shows it as a function of $(M_i^2 - \mu_i^2)^{1/2}$. From Fig. 1, we can see that sizable m_{eff}^N is likely to be obtained by $(M_i^2 - \mu_i^2)^{1/2} \lesssim 1$ GeV. Since $(\tilde{m}_\nu)_{ie}$ appears in the active neutrino mass matrix, i.e. $(m_\nu)_{ee} \simeq \sum_{i=1}^3 (\tilde{m}_\nu)_{ie}$ [see Eq. (8)], $(\tilde{m}_\nu)_{ie}$ is typically $\mathcal{O}(m_\nu)$ without any fine-tuning. However, it can be much larger than $\mathcal{O}(m_\nu)$ with a sufficient fine-tuning, so that m_{eff}^N can be much larger than the naive estimation. We will show numerical results in Sec. 5.

The existence of heavy neutrinos also induce non-standard interactions in the leptonic sector, which correspond to non-unitarity of the PMNS matrix. The deviation from unitarity can be estimated by

$$\epsilon_{\alpha\beta} \equiv \left| \sum_{i=4}^7 U_{\alpha i} U_{\beta i}^* \right| = \left| \delta_{\alpha\beta} - (NN^\dagger)_{\alpha\beta} \right|, \quad (20)$$

where N is the 3×3 non-unitary matrix describing the mixing between the light neutrino mass eigenstates and the $SU(2)_L$ gauge eigenstates, that is, the PMNS matrix. The values of $\epsilon_{\alpha\beta}$ are severely constrained by the combined data from neutrino oscillation data, lepton-flavor-violating decays of charged leptons, non-universality of weak interaction, CKM unitarity bounds, and EW precision data [39]:

$$|\epsilon_{\alpha\beta}| \leq \begin{pmatrix} 2.5 \times 10^{-3} & 2.4 \times 10^{-5} & 2.7 \times 10^{-3} \\ 2.4 \times 10^{-5} & 4.0 \times 10^{-4} & 1.2 \times 10^{-3} \\ 2.7 \times 10^{-3} & 1.2 \times 10^{-3} & 5.6 \times 10^{-3} \end{pmatrix}. \quad (21)$$

The constraint on $\epsilon_{e\mu}$ ($= \epsilon_{\mu e}$), which comes from a constraint on the lepton-flavor-violating muon decay $\mu \rightarrow e\gamma$, is much stronger than the others. Without assuming accidental cancellation or special textures for the neutrino Yukawa coupling matrix, once model parameters are set to satisfy $\epsilon_{e\mu} \leq 2.4 \times 10^{-5}$, the other constraints can be simultaneously satisfied.

4 Higgs mass correction

The heavy neutrinos may lead a sizable Higgs mass correction. In our notation, the Higgs potential is given by $V = \lambda(\Phi^\dagger\Phi)^2 + m_H^2\Phi^\dagger\Phi$, and then, the Higgs mass is obtained by $M_h^2 = -2m_H^2 = (125 \text{ GeV})^2$. Then, the heavy neutrinos contribute the Higgs mass parameter as

$$\begin{aligned}\delta m_H^2 &= -\frac{2}{16\pi^2} \text{Tr}[Y_\nu^\dagger M_N^T M_N Y_\nu] \ln\left(\frac{M_{\text{Pl}}^2}{M_N^2}\right) \\ &= -\frac{4}{16\pi^2 v^2} \text{Tr}[D_M^2 D_X R D_m R^\dagger] \ln\left(\frac{M_{\text{Pl}}^2}{M_N^2}\right),\end{aligned}\quad (22)$$

where we have used Casas-Ibarra parametrization (10), and assumed both M_N and μ_S are diagonal. We have taken cutoff scale as the reduced Planck scale $M_{\text{Pl}} = 2.44 \times 10^{18} \text{ GeV}$. In the last expression of Eq. (22), $D_X \rightarrow D_M$ corresponds to the Higgs mass correction in the type-I seesaw model. Thus, in the inverse seesaw model, the Higgs mass correction can be enhanced by a factor M_N/μ_S compared to the type-I seesaw model.

Since we have assumed that both M_N and μ_S are diagonal, the trace part in Eq. (22) can be simply shown by

$$\text{Tr}[D_M^2 D_X R D_m R^\dagger] = \left(\frac{M_1^4}{\mu_1}, \frac{M_2^4}{\mu_2}, \frac{M_3^4}{\mu_3}\right) \begin{pmatrix} |R_{11}|^2 & |R_{12}|^2 & |R_{13}|^2 \\ |R_{21}|^2 & |R_{22}|^2 & |R_{23}|^2 \\ |R_{31}|^2 & |R_{32}|^2 & |R_{33}|^2 \end{pmatrix} \begin{pmatrix} m_1 \\ m_2 \\ m_3 \end{pmatrix}. \quad (23)$$

In addition, when both M_N and μ_S are degenerate, i.e., $M_N = M_d \mathbf{1}$ and $\mu_S = \mu_d \mathbf{1}$, this trace can be rewritten by

$$\text{Tr}[D_M^2 D_X R D_m R^\dagger] = \frac{M_d^4}{\mu_d} (R_1 m_1 + R_2 m_2 + R_3 m_3), \quad (24)$$

with $R_i \equiv \sum_{j=1}^3 |R_{ji}|^2$, which is obtained by

$$\begin{aligned}R_1 &= |c_{12}|^2 |c_{13}|^2 + (|s_{12}|^2 + |c_{12}|^2 |s_{13}|^2) \cosh(2\text{Im}[\omega_{23}]) + 2\text{Im}[s_{12} c_{12}^* s_{13}^*] \sinh(2\text{Im}[\omega_{23}]), \\ R_2 &= |s_{12}|^2 |c_{13}|^2 + (|c_{12}|^2 + |s_{12}|^2 |s_{13}|^2) \cosh(2\text{Im}[\omega_{23}]) + 2\text{Im}[s_{12} c_{12}^* s_{13}] \sinh(2\text{Im}[\omega_{23}]), \\ R_3 &= |s_{13}|^2 + |c_{13}|^2 \cosh(2\text{Im}[\omega_{23}]).\end{aligned}\quad (25)$$

In this expression, we can see $R_i \geq 1$. This fact is easily understood in two flavor case, in which the number of right-handed neutrinos and sterile neutrinos are two. In the two

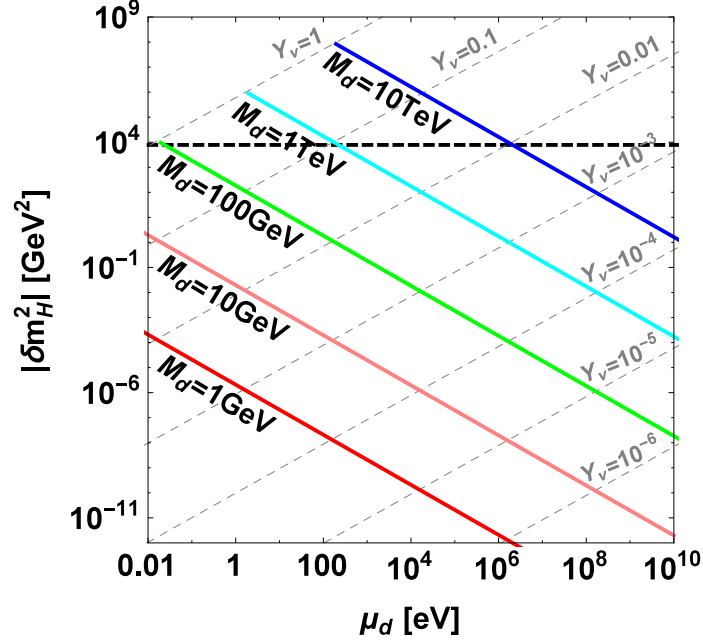


Figure 2: Higgs mass correction as a function of μ_d , which are shown by the red, pink, green, cyan and blue lines for $M_d = 1, 10, 10^2, \dots$, and 10^5 GeV, respectively. The black-dashed line corresponds to $|\delta m_H^2| = M_h^2/2$ with $M_h = 125$ GeV. Typical values of neutrino Yukawa coupling can be estimated by Eq. (6), and they are shown by the gray-dashed lines for $Y_\nu = 1, 10^{-1}, 10^{-2}, \dots$, and 10^{-6} from the upper left to the lower right.

flavor case, the lightest neutrino is massless, and R is expressed by only one complex angle. The normal hierarchy (NH) corresponds to $m_1 = 0$ and $\omega_{12} = \omega_{13} = 0$, which lead $R_2 = R_3 = \cosh(2\text{Im}[\omega_{23}]) \geq 1$. In the same way, the inverted hierarchy (IH) corresponds to $m_3 = 0$ and $\omega_{13} = \omega_{23} = 0$, which lead $R_1 = R_2 = |c_{12}|^2 + |s_{12}|^2 = \cosh(2\text{Im}[\omega_{12}]) \geq 1$.

As a result, the Higgs mass correction has the minimal value:

$$|\delta m_H^2| \geq \frac{4M_d^4}{16\pi^2 v^2 \mu_d} (m_1 + m_2 + m_3) \ln \left(\frac{M_{\text{Pl}}^2}{M_d^2} \right), \quad (26)$$

where the equals sign holds with, e.g., $R = 1$. For the non-degenerate case, M_d is replaced by the heaviest neutrino mass. Figure 2 shows the Higgs mass correction as a function of μ_d , which corresponds to the minimal value of Eq. (26). For reference values, we have considered the NH case, and taken $m_1 = 0$, $m_2 = \sqrt{7.49 \times 10^{-5}} \text{ eV}$ and $m_3 = \sqrt{2.484 \times 10^{-3}} \text{ eV}$ [40]. The red, pink, green, cyan and blue lines show $|\delta m_H^2|$ for $M_d = 1, 10, 10^2, \dots$, and 10^5 GeV, respectively. Using the seesaw relation (6), typical values of neutrino Yukawa coupling can be determined by a function of μ_d with a fixed M_d , which are shown in the gray-dashed lines. From Fig. 2, we can see that the Higgs mass correction becomes larger as μ_d becomes smaller. When μ_d is smaller than 0.1 eV, the inverse seesaw mechanism does not work successfully as shown in Eq. (7). For $\mu_d > 0.1 \text{ eV}$, the heavy neutrino contributions to the Higgs mass become dominant for $M_d \gtrsim 160 \text{ GeV}$.

	$\sin^2 \theta_{12}$	$\sin^2 \theta_{23}$	$\sin^2 \theta_{13}$	$\frac{\Delta m_{21}^2}{10^{-5} \text{eV}^2}$	$\frac{\Delta m_{3\ell}^2}{10^{-3} \text{eV}^2}$
NH	$0.273 \rightarrow 0.349$	$0.390 \rightarrow 0.639$	$0.0187 \rightarrow 0.0250$	$7.02 \rightarrow 8.08$	$2.351 \rightarrow 2.618$
IH	$0.273 \rightarrow 0.349$	$0.400 \rightarrow 0.637$	$0.0190 \rightarrow 0.0251$	$7.02 \rightarrow 8.08$	$2.341 \rightarrow 2.595$

Table 1: Global fit values of neutrino oscillation parameters in 3σ CL range [40]. The mass squared differences are defined by $\Delta m_{21}^2 = m_2^2 - m_1^2$ and $\Delta m_{3\ell}^2 = |m_3^2 - m_\ell^2|$ with $\ell = 1$ and 2 for the NH and the IH cases, respectively. There are no constraints for all CP phases in 3σ CL range.

This fact is much different from the type-I seesaw model, in which $|\delta m_H^2| < M_h^2/2$ for $M_d < 10^6 \text{ GeV}$. Therefore, from the naturalness point of view, inverse seesaw models have to introduce heavy neutrinos more carefully than the type-I seesaw model.

5 Numerical analysis

In this section, we show numerical results of the effective neutrino mass (15) and the Higgs mass correction (22). We focus on the case where M_N and $\mu_N = \mu_S$ are real diagonal matrices and normally hierarchical M_N , i.e., $M_1 < M_2 < M_3$. Actually, even if they are not normally hierarchical, we have found similar conclusions for other hierarchies. In our numerical calculations, we take the input parameters as

$$\begin{aligned}
m_{1(3)} &= [10^{-4} \text{ eV}, 0.07 (0.065) \text{ eV}] \text{ for NH (IH)}, \\
M_i &= [10 \text{ MeV}, 100 \text{ TeV}], \\
\mu_i &= [1 \text{ eV}, 1 \text{ MeV}], \\
\omega_{ij} &= [0, \pi] \times e^{i[0, 2\pi]},
\end{aligned} \tag{27}$$

and neutrino oscillation parameters satisfy the current experimental constraints shown in Table 1. The upper bound of the lightest active neutrino mass is given by the cosmological bound $\sum m_i < 0.23 \text{ eV}$ [41]. In addition, the mixing matrix U satisfies the constraints of the non-unitarity (21). Note that, however, there exist severe constraints in a low M_i region ($M_i \lesssim 2 \text{ GeV}$), which are obtained by π and K peak searches, π , K , D , Z decay searches, and LHC collider searches. They are summarized in Ref. [18], and we also apply their constraints in our analysis.

For the neutrinoless double beta decay, the lightest heavy neutrino mass M_1 is sensitive. Figure 3 shows M_1 dependence of $|m_{\text{eff}}^N|$ with the blue dots, while the red dots show the active neutrino contribution $|m_{\text{eff}}^\nu|$, which does not depend on heavy neutrinos. The cyan and pink dots show the excluded points due to the constraints in Ref. [18] for $|m_{\text{eff}}^N|$ and $|m_{\text{eff}}^\nu|$, respectively. The behavior of $|m_{\text{eff}}^N|$ is the same as Fig. 1, which is expected from our analytical result (18). The heavy neutrino contribution can be much larger than the active neutrino contribution in the range of $M_1 \lesssim 1 \text{ GeV}$.

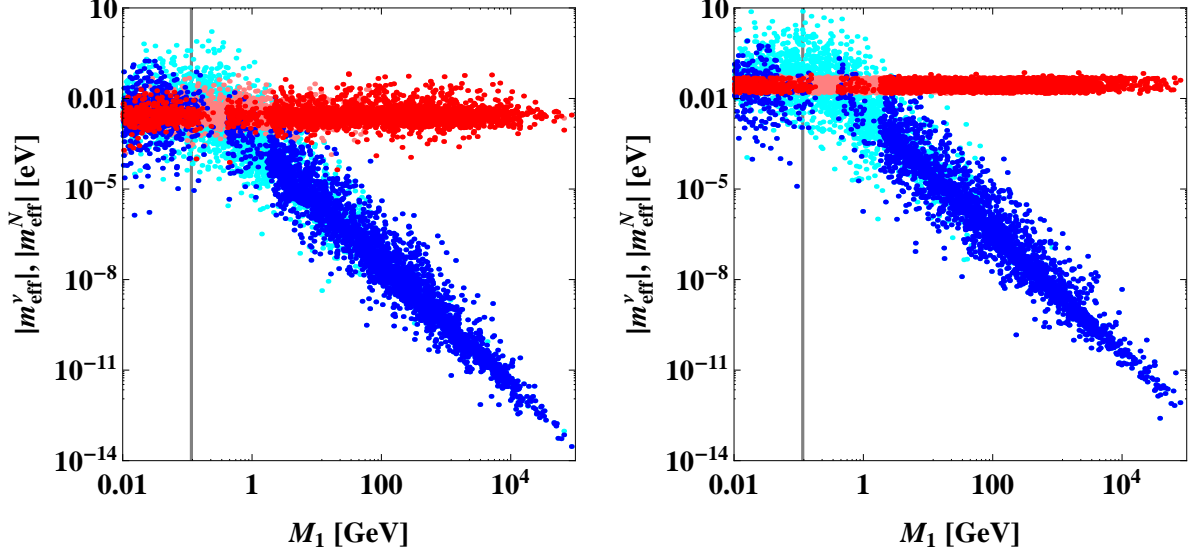


Figure 3: Heavy neutrino mass dependence of $|m_{\text{eff}}^N|$ (blue dots). The red dots show $|m_{\text{eff}}^\nu|$, which does not depend on heavy neutrinos. The cyan and pink dots show the excluded points due to the constraints in Ref. [18] for $|m_{\text{eff}}^N|$ and $|m_{\text{eff}}^\nu|$, respectively. The vertical line shows $\sqrt{\bar{p}^2/3}$ with $\sqrt{\bar{p}^2} = 200$ MeV. The left and right panels correspond to the NH and the IH cases, respectively.

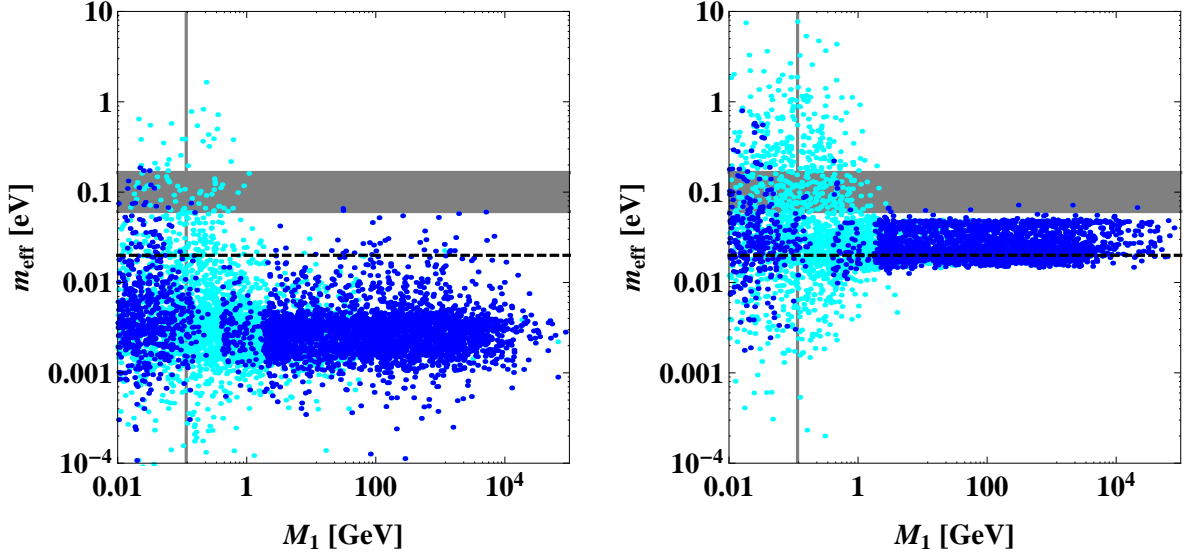


Figure 4: Heavy neutrino mass dependence of m_{eff} (blue dots). The cyan dots show the excluded points due to the constraints in Ref. [18]. The gray band and the black-dashed line show the current upper bound $m_{\text{eff}} < (61 - 165)$ meV and the future sensitivity $m_{\text{eff}} < 0.02$ eV, respectively. The vertical line shows $\sqrt{\bar{p}^2/3}$ with $\sqrt{\bar{p}^2} = 200$ MeV. The left and right panels correspond to the NH and the IH cases, respectively.

Figure 4 shows M_1 dependence of m_{eff} (blue dots). The cyan dots show the excluded points due to the constraints in Ref. [18]. The gray band and the black-dashed line corre-

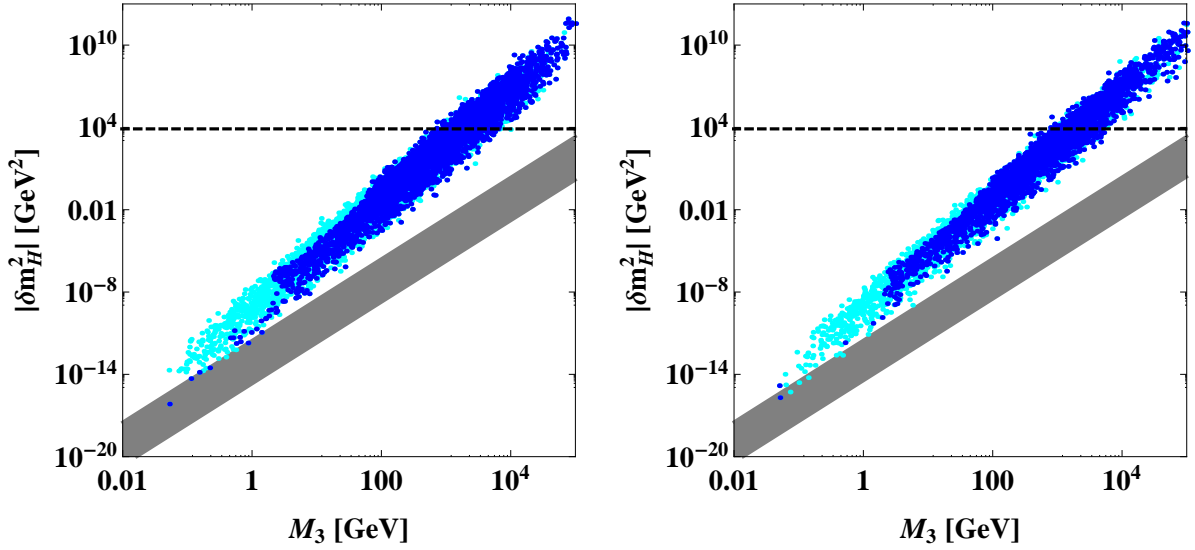


Figure 5: Heavy neutrino mass dependence of the Higgs mass correction (blue dots). The cyan dots show the excluded points due to the constraints in Ref. [18]. The gray band and the black-dashed line show the type-I seesaw case, and $|\delta m_H^2| = M_h^2/2$ with $M_h = 125$ GeV, respectively. The left and right panels correspond to the NH and the IH cases, respectively.

sponds to the current upper bound $m_{\text{eff}} < (61 - 165)$ meV obtained by the KamLAND-Zen experiment [13] and their future sensitivity $m_{\text{eff}} < 0.02$ eV, respectively. For $M_1 > 1$ GeV, the heavy neutrino contribution is strongly suppressed, and thus, there are almost no points above the current upper bound. Note that there exists $m_{\text{eff}} < |m_{\text{eff}}^\nu|$ region, since m_{eff}^ν and m_{eff}^N can be canceled each other. Thus, the IH case is not completely excluded.

For the Higgs mass correction, the heaviest heavy neutrino mass M_3 is sensitive. Figure 5 shows M_3 dependence of $|\delta m_H^2|$ (blue dots). The cyan dots show the excluded points due to the constraints in Ref. [18]. The gray band shows the type-I seesaw case, and the black-dashed line corresponds to $|\delta m_H^2| = M_h^2/2$ with $M_h = 125$ GeV. The minimal value of Higgs mass correction can be predicted by Eq. (26). For the maximal value of $\text{Im}[\omega_{ij}] = \omega_{\text{max}}$ (in our numerical analysis $\omega_{\text{max}} = \pi$), the maximal value of Higgs mass correction is approximately given by the minimal value times $\cosh(2\omega_{\text{max}})$. There is no difference between the NH and the IH cases. Note that $M_i \gtrsim 10^5$ GeV, which equivalently corresponds to $Y_\nu \gtrsim 1$, is excluded by the constraint from lepton flavor violations. If we allow μ_i to take a larger value than 1 MeV, Y_ν can be smaller than before, and then, there exist allowed regions for $M_i \gtrsim 10^5$ GeV. However, since such a large μ_i means a large lepton number violation, it conflicts the naturalness. Thus, we have imposed $\mu_i \leq 1$ MeV.

As we expected in Sec. 4, the Higgs mass correction can be larger than the Higgs mass for $M_3 \gtrsim 1$ TeV, while for $M_3 \gtrsim 10^6$ GeV in the type-I seesaw model. This difference

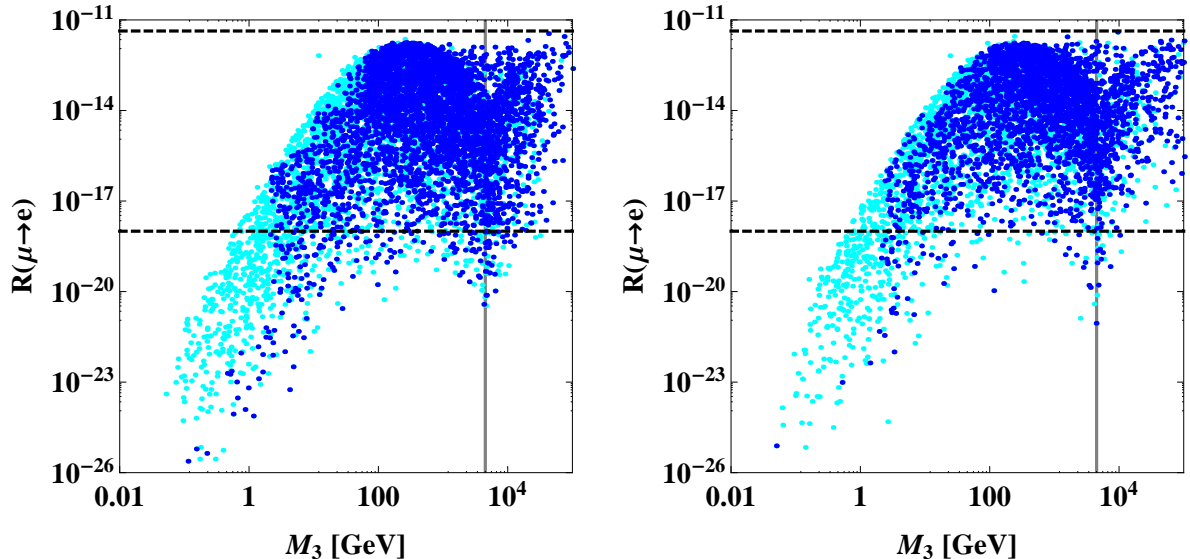


Figure 6: The rate of $\mu \rightarrow e$ conversion in Titanium (blue dots). The cyan dots show the excluded points due to the constraints in Ref. [18]. The black-dashed lines correspond to the current upper bound $R_{\mu \rightarrow e} < 4.3 \times 10^{-12}$ and the future sensitivity of PRISM experiment $R_{\mu \rightarrow e} < 10^{-18}$. The vertical line shows $M_3 = 4.5$ TeV, at which the contribution of the $\mu \rightarrow e$ conversion vanishes. The left and right panels correspond to the NH and the IH cases, respectively.

corresponds to the difference of size of neutrino Yukawa coupling, that is, in the inverse seesaw model Y_ν is much larger compared with the type-I seesaw case. The large Y_ν causes a large mixing between left-handed neutrinos and gauge-singlet neutrinos. However, such a large mixing can be severely constrained by future experiments of the lepton flavor violation. In particular, a future experiment of $\mu \rightarrow e$ conversion at PRISM can give the strongest constraint.

Figure 6 shows the rate of $\mu \rightarrow e$ conversion in Titanium (blue dots), which has been calculated as in Appendix A. The cyan dots show the excluded points due to the constraints in Ref. [18]. The black-dashed line corresponds to the future sensitivity of PRISM experiment $R_{\mu \rightarrow e} < 10^{-18}$ [24], while the current upper bound is $R_{\mu \rightarrow e} < 4.3 \times 10^{-12}$ [42]. For Titanium, the $\mu \rightarrow e$ conversion rate vanishes at $M_i \simeq 4.5$ TeV. Since the vanishing point is the different for the various nuclei, the experiment using Titanium can be complemented by experiments using other nuclei. In addition, the low mass region $M_i \lesssim 140$ MeV may be excluded by constraints coming from the big bang nucleosynthesis [43]. Therefore, we can expect the inverse seesaw model is highly testable, i.e., future experiments of neutrinoless double beta decay and $\mu \rightarrow e$ conversion can search the low mass region $M_i \lesssim 1$ GeV and the high mass region $M_i \gtrsim 1$ GeV, respectively.²

² If we allow μ_i to take a larger value than 1 MeV, there is more allowed region which has a smaller Y_ν . Actually, the BAU can be explained only in such a parameter space [35], although it is not preferred

6 Summary

We focus on the (3, 3) inverse seesaw model, in which the number of both right-handed neutrinos and sterile neutrinos are three. We have investigated heavy neutrino contributions for the neutrinoless double beta decay. Its rate is proportional to the effective neutrino mass, and it is useful to estimate contributions from the heavy neutrinos. We have found an analytic form of the heavy neutrino contribution to the effective neutrino mass. It is strongly suppressed for a large heavy-neutrino mass $\gtrsim 1 \text{ GeV}$, while, in $\sim 0.1 \text{ GeV}$ region, it can be enhanced by ten times or more than the active neutrino contribution alone. We have also investigated the Higgs mass correction coming from the heavy neutrinos, and found the minimal value of Higgs mass correction is determined for a given heavy neutrino mass, which is usually larger than the type-I seesaw case. Then, we have shown numerical results of heavy neutrino contributions to the effective neutrino mass and the Higgs mass correction. As a result, we have found that almost all parameter space of the inverse seesaw model can be complementarily searched: the low mass region $M_i \lesssim 1 \text{ GeV}$ and the high mass region $M_i \gtrsim 1 \text{ GeV}$ can be searched by future experiments of neutrinoless double beta decay and $\mu \rightarrow e$ conversion, respectively.

Acknowledgment

This work is partially supported by Scientific Grants by the Ministry of Education, Culture, Sports, Science and Technology of Japan (Nos. 24540272, 26247038, 15H01037, 16H00871, and 16H02189). The work of Y. Y. is supported by Research Fellowships of the Japan Society for the Promotion of Science for Young Scientists (Grants No. 26·2428).

Appendix

A $\mu \rightarrow e$ conversion rate

Due to the existence of the heavy neutrinos, violation of charged lepton number arises at the one loop level. $\mu \rightarrow e$ conversion is induced by a series of gauge boson mediated diagrams. Its rate is calculated by [44]

$$R_{\mu \rightarrow e} \simeq \frac{G_F^2 \alpha_W^2 \alpha^3 m_\mu^5}{8\pi^4 \Gamma_{\text{capt}}} \frac{Z_{\text{eff}}^4}{Z} F_p^2 \left| \sum_{i=1}^9 [(A+Z) F_u(x_i) + (2A-Z) F_d(x_i)] U_{ei} U_{\mu i}^* \right|^2. \quad (28)$$

where $\alpha_W = g_2^2/(4\pi)$, $\alpha = e^2/(4\pi)$, $s_W = \sin \theta_W$ is the Weinberg angle, G_F is the Fermi constant, and m_μ is the muon mass. The other constant parameters depend on a nuclei from the naturalness point of view.

Nucleus ${}^A_Z\text{N}$	Z_{eff}	$ F_p(-m_\mu^2) $	$\Gamma_{\text{capt}} (10^6 s^{-1})$
${}^{27}_{13}\text{Al}$	11.5	0.64	0.7054
${}^{48}_{22}\text{Ti}$	17.6	0.54	2.59
${}^{197}_{79}\text{Au}$	33.5	0.16	13.07
${}^{208}_{82}\text{Pb}$	34.0	0.15	13.45

Table 2: Nuclear form factors and capture rates.

information which is used in experiments. A is the mass number, Z (Z_{eff}) is the (effective) atomic number, F_p is a nuclear form factor, and Γ_{capt} is the capture rate. These values are given in Table 2 [44].

$F_u(x_i)$ and $F_d(x_i)$ are functions of $x_i \equiv m_i^2/M_W^2$ given as

$$\begin{aligned} \tilde{F}_u(x) = & \frac{2}{3}s_W^2 \left[F_\gamma(x) - F_Z(x) - 2G_Z(0, x) \right] \\ & + \frac{1}{4} \left[F_Z(x) + 2G_Z(0, x) + F_{Box}(0, x) - F_{Box}(0, 0) \right], \end{aligned} \quad (29)$$

$$\begin{aligned} \tilde{F}_d(x) = & -\frac{1}{3}s_W^2 \left[F_\gamma(x) - F_Z(x) - 2G_Z(0, x) \right] \\ & - \frac{1}{4} \left[F_Z(x) + 2G_Z(0, x) - F_{XBox}(0, x) + F_{XBox}(0, 0) \right], \end{aligned} \quad (30)$$

$$F_u(x) = \tilde{F}_u(x) + \frac{2}{3}s_W^2 G_\gamma(x), \quad (31)$$

$$F_d(x) = \tilde{F}_d(x) - \frac{1}{3}s_W^2 G_\gamma(x). \quad (32)$$

The loop functions are

$$F_\gamma(x) = \frac{x(7x^2 - x - 12)}{12(1-x)^3} - \frac{x^2(x^2 - 10x + 12)}{6(1-x)^4} \ln x, \quad (33)$$

$$G_\gamma(x) = -\frac{x(2x^2 + 5x - 1)}{4(1-x)^3} - \frac{3x^3}{2(1-x)^4} \ln x, \quad (34)$$

$$F_Z(x) = -\frac{5x}{2(1-x)} - \frac{5x^2}{2(1-x)^2} \ln x, \quad (35)$$

$$G_Z(x, y) = -\frac{1}{2(x-y)} \left[\frac{x^2(1-y)}{1-x} \ln x - \frac{y^2(1-x)}{1-y} \ln y \right], \quad (36)$$

$$\begin{aligned} F_{Box}(x, y) = & \frac{1}{x-y} \left\{ \left(4 + \frac{xy}{4} \right) \left[\frac{1}{1-x} + \frac{x^2}{(1-x)^2} \ln x - \frac{1}{1-y} - \frac{y^2}{(1-y)^2} \ln y \right] \right. \\ & \left. - 2xy \left[\frac{1}{1-x} + \frac{x}{(1-x)^2} \ln x - \frac{1}{1-y} - \frac{y}{(1-y)^2} \ln y \right] \right\}, \end{aligned} \quad (37)$$

$$\begin{aligned} F_{XBox}(x, y) = & \frac{-1}{x-y} \left\{ \left(1 + \frac{xy}{4} \right) \left[\frac{1}{1-x} + \frac{x^2}{(1-x)^2} \ln x - \frac{1}{1-y} - \frac{y^2}{(1-y)^2} \ln y \right] \right. \\ & \left. - 2xy \left[\frac{1}{1-x} + \frac{x}{(1-x)^2} \ln x - \frac{1}{1-y} - \frac{y}{(1-y)^2} \ln y \right] \right\}, \end{aligned} \quad (38)$$

with the limiting values

$$G_Z(0, x) = -\frac{x}{2(1-x)} \ln x, \quad (39)$$

$$F_{Box}(0, x) = \frac{4}{1-x} + \frac{4x}{(1-x)^2} \ln x, \quad F_{XBox}(0, x) = -\frac{1}{1-x} - \frac{x}{(1-x)^2} \ln x. \quad (40)$$

As a result, Eqs. (31) and (32) are given by

$$F_u(x) = \frac{1}{72(1-x)^4} \left[(1-x)x \{ 27(1-x)^2 + 4s_W^2(31x^2 - 76x + 21) \} \right. \\ \left. + x \{ 27(2-x)(1-x)^2 + 8s_W^2(8x^3 - 11x^2 - 15x + 6) \} \ln x \right], \quad (41)$$

$$F_d(x) = \frac{1}{72(1-x)^4} \left[(1-x)x \{ 27(1-x)^2 - 2s_W^2(31x^2 - 76x + 21) \} \right. \\ \left. + x \{ 27x(1-x)^2 - 4s_W^2(8x^3 - 11x^2 - 15x + 6) \} \ln x \right]. \quad (42)$$

References

- [1] P. Minkowski, Phys. Lett. B **67**, 421 (1977) doi:10.1016/0370-2693(77)90435-X;
T. Yanagida, Conf. Proc. C **7902131**, 95 (1979);
M. Gell-Mann, P. Ramond and R. Slansky, Conf. Proc. C **790927**, 315 (1979) [arXiv:1306.4669 [hep-th]];
R. N. Mohapatra and G. Senjanovic, Phys. Rev. Lett. **44**, 912 (1980) doi:10.1103/PhysRevLett.44.912;
J. Schechter and J. W. F. Valle, Phys. Rev. D **22**, 2227 (1980); Phys. Rev. D **25** 774 (1982).
- [2] T. A. Mueller *et al.*, Phys. Rev. C **83**, 054615 (2011) doi:10.1103/PhysRevC.83.054615 [arXiv:1101.2663 [hep-ex]].
- [3] P. Huber, Phys. Rev. C **84**, 024617 (2011) Erratum: [Phys. Rev. C **85**, 029901 (2012)] doi:10.1103/PhysRevC.85.029901, 10.1103/PhysRevC.84.024617 [arXiv:1106.0687 [hep-ph]].
- [4] G. Mention, M. Fechner, T. Lasserre, T. A. Mueller, D. Lhuillier, M. Cribier and A. Letourneau, Phys. Rev. D **83**, 073006 (2011) doi:10.1103/PhysRevD.83.073006 [arXiv:1101.2755 [hep-ex]].
- [5] A. Aguilar-Arevalo *et al.* [LSND Collaboration], Phys. Rev. D **64**, 112007 (2001) doi:10.1103/PhysRevD.64.112007 [hep-ex/0104049].
- [6] A. A. Aguilar-Arevalo *et al.* [MiniBooNE Collaboration], Phys. Rev. Lett. **98**, 231801 (2007) doi:10.1103/PhysRevLett.98.231801 [arXiv:0704.1500 [hep-ex]].

- [7] A. A. Aguilar-Arevalo *et al.* [MiniBooNE Collaboration], Phys. Rev. Lett. **105**, 181801 (2010) doi:10.1103/PhysRevLett.105.181801 [arXiv:1007.1150 [hep-ex]].
- [8] A. A. Aguilar-Arevalo *et al.* [MiniBooNE Collaboration], Phys. Rev. Lett. **110**, 161801 (2013) doi:10.1103/PhysRevLett.110.161801 [arXiv:1207.4809 [hep-ex], arXiv:1303.2588 [hep-ex]].
- [9] M. A. Acero, C. Giunti and M. Laveder, Phys. Rev. D **78**, 073009 (2008) doi:10.1103/PhysRevD.78.073009 [arXiv:0711.4222 [hep-ph]].
- [10] C. Giunti and M. Laveder, Phys. Rev. C **83**, 065504 (2011) doi:10.1103/PhysRevC.83.065504 [arXiv:1006.3244 [hep-ph]].
- [11] M. Drewes, Int. J. Mod. Phys. E **22**, 1330019 (2013) doi:10.1142/S0218301313300191 [arXiv:1303.6912 [hep-ph]].
- [12] M. Fukugita and T. Yanagida, Phys. Lett. B **174**, 45 (1986). doi:10.1016/0370-2693(86)91126-3
- [13] A. Gando *et al.* [KamLAND-Zen Collaboration], arXiv:1605.02889 [hep-ex].
- [14] G. 't Hooft, NATO Sci. Ser. B **59**, 135 (1980).
- [15] D. Wyler and L. Wolfenstein, Nucl. Phys. B **218**, 205 (1983). doi:10.1016/0550-3213(83)90482-0
- [16] R. N. Mohapatra and J. W. F. Valle, Phys. Rev. D **34**, 1642 (1986). doi:10.1103/PhysRevD.34.1642
- [17] M. C. Gonzalez-Garcia and J. W. F. Valle, Phys. Lett. B **216**, 360 (1989). doi:10.1016/0370-2693(89)91131-3
- [18] A. Atre, T. Han, S. Pascoli and B. Zhang, JHEP **0905**, 030 (2009) doi:10.1088/1126-6708/2009/05/030 [arXiv:0901.3589 [hep-ph]].
- [19] M. Drewes and B. Garbrecht, arXiv:1502.00477 [hep-ph].
- [20] P. S. B. Dev, A. Pilaftsis and U. k. Yang, Phys. Rev. Lett. **112**, no. 8, 081801 (2014) doi:10.1103/PhysRevLett.112.081801 [arXiv:1308.2209 [hep-ph]].
- [21] A. Das, P. S. Bhupal Dev and N. Okada, Phys. Lett. B **735**, 364 (2014) doi:10.1016/j.physletb.2014.06.058 [arXiv:1405.0177 [hep-ph]].
- [22] A. M. Baldini *et al.*, arXiv:1301.7225 [physics.ins-det].

- [23] A. Blondel *et al.*, arXiv:1301.6113 [physics.ins-det].
- [24] R. J. Barlow, Nucl. Phys. Proc. Suppl. **218**, 44 (2011).
doi:10.1016/j.nuclphysbps.2011.06.009
- [25] C. Y. Chen and P. S. B. Dev, Phys. Rev. D **85**, 093018 (2012)
doi:10.1103/PhysRevD.85.093018 [arXiv:1112.6419 [hep-ph]].
- [26] A. Das and N. Okada, Phys. Rev. D **88**, 113001 (2013)
doi:10.1103/PhysRevD.88.113001 [arXiv:1207.3734 [hep-ph]].
- [27] E. Arganda, M. J. Herrero, X. Marcano and C. Weiland, Phys. Rev. D **91**, no. 1, 015001 (2015) doi:10.1103/PhysRevD.91.015001 [arXiv:1405.4300 [hep-ph]].
- [28] F. F. Deppisch, P. S. Bhupal Dev and A. Pilaftsis, New J. Phys. **17**, no. 7, 075019 (2015) doi:10.1088/1367-2630/17/7/075019 [arXiv:1502.06541 [hep-ph]].
- [29] T. Golling *et al.*, arXiv:1606.00947 [hep-ph].
- [30] S. S. C. Law and K. L. McDonald, Phys. Rev. D **87**, no. 11, 113003 (2013)
doi:10.1103/PhysRevD.87.113003 [arXiv:1303.4887 [hep-ph]].
- [31] Z. Maki, M. Nakagawa and S. Sakata, Prog. Theor. Phys. **28** (1962) 870;
- [32] B. Pontecorvo, Sov. Phys. JETP **26** (1968) 984 [Zh. Eksp. Teor. Fiz. **53** (1967) 1717].
- [33] J. A. Casas and A. Ibarra, Nucl. Phys. B **618**, 171 (2001) doi:10.1016/S0550-3213(01)00475-8 [hep-ph/0103065].
- [34] E. K. Akhmedov, V. A. Rubakov and A. Y. Smirnov, Phys. Rev. Lett. **81**, 1359 (1998) doi:10.1103/PhysRevLett.81.1359 [hep-ph/9803255].
- [35] A. Abada, G. Arcadi, V. Domcke and M. Lucente, JCAP **1511**, no. 11, 041 (2015)
doi:10.1088/1475-7516/2015/11/041 [arXiv:1507.06215 [hep-ph]].
- [36] J. Kopp, P. A. N. Machado, M. Maltoni and T. Schwetz, JHEP **1305**, 050 (2013)
doi:10.1007/JHEP05(2013)050 [arXiv:1303.3011 [hep-ph]].
- [37] A. Abada, G. Arcadi and M. Lucente, JCAP **1410**, 001 (2014) doi:10.1088/1475-7516/2014/10/001 [arXiv:1406.6556 [hep-ph]].
- [38] A. Abada and M. Lucente, Nucl. Phys. B **885**, 651 (2014)
doi:10.1016/j.nuclphysb.2014.06.003 [arXiv:1401.1507 [hep-ph]].

- [39] E. Fernandez-Martinez, J. Hernandez-Garcia and J. Lopez-Pavon, arXiv:1605.08774 [hep-ph].
- [40] M. C. Gonzalez-Garcia, M. Maltoni and T. Schwetz, JHEP **1411**, 052 (2014) doi:10.1007/JHEP11(2014)052 [arXiv:1409.5439 [hep-ph]].
- [41] P. A. R. Ade *et al.* [Planck Collaboration], arXiv:1502.01589 [astro-ph.CO].
- [42] C. Dohmen *et al.* [SINDRUM II Collaboration], Phys. Lett. B **317**, 631 (1993). doi:10.1016/0370-2693(93)91383-X
- [43] L. Canetti, M. Drewes, T. Frossard and M. Shaposhnikov, Phys. Rev. D **87**, 093006 (2013) doi:10.1103/PhysRevD.87.093006 [arXiv:1208.4607 [hep-ph]].
- [44] R. Alonso, M. Dhen, M. B. Gavela and T. Hambye, JHEP **1301**, 118 (2013) doi:10.1007/JHEP01(2013)118 [arXiv:1209.2679 [hep-ph]].